Kinetic and Structural Analysis of Enzyme Sliding on a Substrate: Multiple Attack in β-Amylase‡

Kazuhiko Ishikawa,*,§ Hiroshi Nakatani,|| Yoshio Katsuya,⊥,# and Chikafusa Fukazawa△,○

National Institute of Advanced Industrial Science and Technology (AIST), 1-8-31 Midorigaoka, Ikeda, Osaka 563-8577, Japan, Faculty of Agriculture, Kyoto University, Kitashirakawa, Kyoto 606-8502, Japan, Hyogo Prefectural Institute of Industrial Research, 3-1-12 Yukihira-cho, Suma-ku, Kobe, Hyogo 654-0037, Japan, and Genetic Engineering Laboratory, National Food Research Institute, Kannondai, Tsukuba Science City, Ibaraki 305-8642, Japan

Received August 8, 2006; Revised Manuscript Received November 6, 2006

ABSTRACT: β-Amylase (EC 3.2.1.2) is starch-hydrolyzing exo-type enzyme that can catalyze the successive liberation of β-maltose from the nonreducing ends of α-1,4-linked glucopyranosyl polymers. There is a well-known phenomenon called multiple or repetitive attack where the enzyme releases several maltose molecules in a single enzyme−substrate complex. In order to understand it further, we examined the β-amylase-catalyzed reaction using maltooligosaccharides. The Monte Carlo method was applied for simulation of the β-amylase-catalyzed reaction including the multiple attack mechanism. Through site-directed mutagenesis, we have successfully prepared a mutant enzyme which may be simulated as a multiple attack action reduced one with retaining significant hydrolytic activity. From the results of X-ray structure analysis of the mutant enzyme, it was clarified that one carboxyl residue plays a very important role in the multiple attack. The multiple attack action needs the force of enzyme sliding on the substrate. In addition, it is important for the multiple attack that the enzyme and substrate have the characteristics of a stable productive substrate−enzyme complex through a hydrogen bond between the nonreducing end of the substrate and the carboxyl residue of the enzyme.

In the case of high molecular substrates like amylose and amylopectin, some amylases exhibit a unique hydrolytic phenomenon called multiple attack; i.e., the enzyme releases several products effectively from a single enzyme−substrate complex without dissociation through multiple or repetitive attack involving many branching reaction paths (*1*−*7*). The same phenomenon was observed for other exo-type β-1,4-D-glucanases (cellulase and chitinase) (*8*−*11*). This phenomenon is important for the enzymes to attack the substrate effectively. Similar phenomena have also been observed for DNA-related proteins sliding on nucleotide chains (*12*−*14*). The mechanism for DNA-related proteins is speculated to be related to the weak electrostatic interaction between DNA and the binding site of a protein molecule. β-Amylase (EC 3.2.1.2) is an exo-type starch-hydrolyzing enzyme that releases maltose. The active site is located in the cleft of the enzyme, and the substrate binding site at the nonreducing end is blocked by a part of the β-barrel structure of the enzyme (*15*−*17*). Most β-amylases have the common $(\alpha/\beta)_8$-barrel structure and some conserved amino acid residues (*18*, *19*). Furthermore, the structures of their active site are similar to one another (*19*−*21*), and two conserved Glu residues have been assigned as the catalytic residues of β-amylase (*15*, *21*, *22*). The Monte Carlo method is a simple and new method that can be applied for simulation and analysis of the complicated β-amylase-catalyzed reaction including the multiple attack mechanism (*23*, *24*). In this study, we first tried to clarify the critical amino acid residue and elucidate the molecular mechanism of the sliding through X-ray structural analysis and Monte Carlo simulation.

MATERIALS AND METHODS

Materials. Native β-amylase (n-SBA)[1] was purified from soybeans. Main isozymes (PI = 5.22−5.32), isozyme 2 (PI = 5.09), and isozyme 3 (PI = 4.97) were prepared as reported previously (*25*, *26*). Recombinant soybean β-amylase (r-SBA) was prepared using *Escherichia coli* (*22*, *25*). The preparation and purification of the mutant SBAs were performed by the method previously described (*22*). The substrate maltoheptaose (G7) of the enzyme was purchased from Seikagaku Corp. (Tokyo, Japan).

Enzyme Assays. The hydrolytic activity of SBA was examined by the method described previously (*22*, *25*). The activity was defined as the initial velocity of the decrease of the substrate, G7. One unit of the enzyme is defined as the initial velocity for an increase of 1 μM maltose per 1 min.

‡ The structure factors and refined coordinates of W55R have been deposited with Protein Data Bank, accession code 2DQX.

* To whom correspondence should be addressed. Phone: +81-72-751-9526. Fax: +81-72-751-9628. E-mail: kazu-ishikawa@aist.go.jp.

§ National Institute of Advanced Industrial Science and Technology.

|| Kyoto University.

⊥ Hyogo Prefectural Institute of Industrial Research.

Present address: SPring-8 Service Co. Ltd., 1-1-1 Kouto, Sayo-cho, Sayo-gun, Hyogo 679-5198, Japan.

△ National Food Research Institute.

○ Present address: Division of Research and Development, Kume Quality Products Co., 1194-1, Takagaki-cho, Hitachi-Ohta City, Ibaraki 313-0113, Japan.

[1] Abbreviations: SBA, β-amylase from soybean; G7, maltoheptaose; G5, maltopentaose; G3, maltotriose; G2, maltose; G (Glc), glucose.

10.1021/bi061605w CCC: $37.00
Published on Web 12/21/2006

Analysis of the Multiple Attack Action of SBA. G7 was used as the substrate for analysis of the multiple attack. The enzyme reaction was carried out in 20 mM sodium acetate buffer, pH 5.7, using 0.2% (1.74 mM) of G7 at 37 °C. At appropriate times, the reaction was stopped with 0.2 N HCl, and the products were measured with HPLC equipped with a TSK-Gel G-OLIGO-PW column (Toyosoda, Tokyo, Japan) and an RID-6A refractive index detector (Shimazu, Kyoto, Japan). Through analysis of the product from G7, the degree of multiple attack of SBA was examined, as reported previously (*23*, *24*). From one molecule of G7, two molecules of maltose (G2) and one molecule of maltotriose (G3) are produced by SBA as the final products. G3 is not hydrolyzed by SBA. Therefore, the degree of reaction was defined as $[G2]/2G7]_0$. $[G7]_0$ is the initial concentration of G7. During the reaction, the degree of reaction changed from 0 to 1. The amounts of other products were expressed as normalized values divided by the initial amount of the substrate, $[G7]_0$. A figure in which the abscissa and ordinate represent the degree of reaction and the normalized amounts of products, respectively, shows the action pattern of β-amylase (*23*, *24*). This plot is independent of the concentration of enzymes and/or substrates.

Model of the Multiple Attack Mechanism and Its Simulation. The experimental data for product distribution from the beginning to the end of the β-amylase reaction were analyzed with the Monte Carlo simulation (*24*). The model assumes only a single enzyme molecule and 10^5 substrate molecules. The reaction progresses with probabilities and random numbers, as shown in Figure 1. The degree of reaction is represented as the amount of G2 in place of the time course. The best-fit parameters (P0 and P5/P7) were estimated by comparison with experimental data by means of the previous paper (*24*), changing independently P0 and P5/P7 values to reach the minimum of error sum between all experimental and theoretical values, where P0, P5, and P7 are the probabilities shown in the legends of Figure 1. The uncertainty limit was ±0.01. The active site of SBA consists of six subsites, unlike five subsites of sweet potato β-amylase (*1*, *24*). Practical procedures for computer simulation are coded and compiled by Microsoft Visual Basic, as described previously (*24*).

Crystal Structure of Mutant SBA. Crystals of the mutant SBA was prepared at 4 °C by the same method as previously described (*21*). Each crystal was completely grown to a size of about 0.06 × 0.08 × 0.06 mm within 60 days. The crystal was soaked in 0.1 M sodium acetate buffer (pH 5.4) containing 1 mM EDTA, 50% saturated ammonium sulfate, and 20% ethylene glycol for 5 min before X-ray diffraction data collection. The X-ray diffraction data were collected at the beamline BL24XU in SPring8 (Harima, Hyogo, Japan). Data were collected with a Rigaku R-AXIS4 image plate detector at 100 K. The crystal diffracted the X-ray to 2.2 Å resolution and was stable during 12 h for 56 oscillation frames. The crystals belong to the space group $P3_121$ with unit cell dimensions of $a = b = 85.05$ Å and $c = 145.03$ Å. These cell parameters are different from the values of n-SBA with 0.19% and 1.14%, respectively (*16*). The collected images were processed with Rigaku Process packages. Data from different frames were integrated separately and then merged together (R_{merge} = 7.4%). The initial phase was calculated using the coordinate from the protein structure of n-SBA (1WDP) (*16*). The model was rebuilt using the Turbo-Frodo program (*27*), and the structure was refined using the program CNS (*28*). Water molecules were incorporated from the $2|F_o| - |F_c|$ map interpretation. The final model contains 490 amino acids (residues 6−495) and 327 water molecules. The final *R*-factor and R_{free} factor calculated for the randomly separated 5% data were 20.5% and 25.2%, respectively. Table 3 summarizes the data collection and statistics.

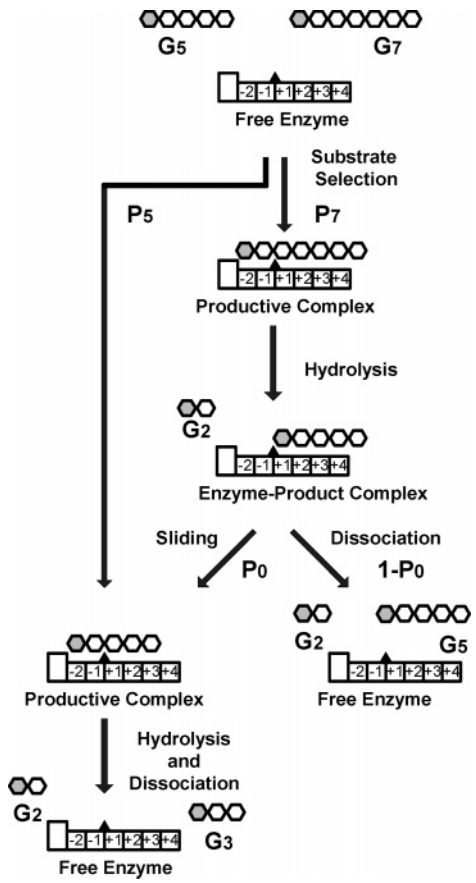

FIGURE 1: Simulation model of the multiple attack (sliding) mechanism of SBA. The enzyme shows the active site of SBA. The catalytic site is indicated as a solid triangle between subsite −1 and +1. Subsites are numbered from the catalytic site. The nonreducing end of the substrate binding site is indicated as subsite −2. Hexagons are glucose residues bound with α-1,4 bonds; the shadowed hexagon is the nonreducing end glucose of the oligosaccharides. The box at the left side of subsite −2 is the block producing only G2 from productive binding mode. No monomer (glucose; G) is produced from SBA. The probability of producing G2 after rearrangement from the enzyme−product complex to the productive complex is shown as P0. The probability of releasing the product is 1 − P0. The probability of forming a productive complex with G5 and G7 is shown as P5 and P7, respectively (P5 + P7 = 1).

RESULTS

In previous kinetical and structural studies of soybean β-amylase (SBA), it was revealed that SBA has main six subsites and that its active center is between subsites −1 and +1 in which active residues Glu186 and Glu380 are located (Figure 1) (*15*, *16*, *22*). SBA has several additional substrate binding sites around Leu383 that can bind cyclodextrins (CDs). It has been speculated that this additional binding site and the flexible loops located (96−103 and 340−346) around the active site play an important role in the

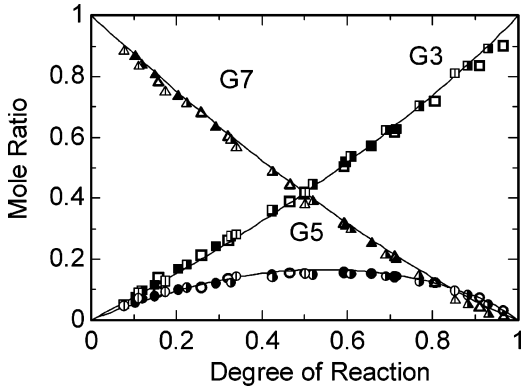

FIGURE 2: Experimental and simulation data for the distribution of products (G5 and G3) from G7 with n- and r-SBAs. The horizontal coordinate is the degree of reaction defined by the relative amount of dimer produced. The vertical coordinate is the mole ratio normalized as to G7. Experimental points are G3 (square), G5 (circle), and G7 (triangle). □, ○, and △ are the data for the main isozyme of n-SBA (54.8 milliunits/mL). ■, ●, and ▲ are the data for isozyme 2 of n-SBA (3.34 milliunits/mL). The half-filled square, circle, and triangle are the data for main isozyme 3 of n-SBA (20.6 milliunits/mL). The square, circle, and triangle with a vertical line are the data for r-SBA (54.8 milliunits/mL). Solid lines are best-fitted simulated data using P0 = 0.55 and (P5/P7) = 1.00 (Figure 1).

multiple attack action (*29*−*31*). In the case of multiple attack of SBA, the oligosaccharide product from the enzyme−product (E−P) complex has to slide to the nonreducing end substrate binding site after releasing maltose (G2) (*1*, *2*, *24*, *31*), as shown in Figure 1. The enzyme and product in the transient stable E−P complex must slide for the multiple attack (Figure 1), as speculated previously (*10*, *29*). Furthermore, after sliding, stabilization of the productive complex is necessary for the multiple attack (sliding pathway, P0) (Figure 1). We assumed that Asp53 and His93 contributing the hydrogen bond between the enzyme and the nonreducing end substrate as subsite −2 are important (Figure 1) (*16*). In this study, we focused on the carboxyl residue of Asp53 located at the nonreducing end of substrate binding site. By removing and changing the position of the carboxyl residue of Asp53 by the protein engineering method, we examined the action pattern of native and mutant SBAs in detail.

Product Distribution from G7 by SBA. In the case of the native SBA (n-SBA) reaction, significant maltotriose (G3) product was observed at the first stage of the reaction with an oligosaccharide substrate of which chain length number was odd. G3 is not hydrolyzed by β-amylase. This result shows the multiple attack action of the β-amylase. The mechanism was observed at first in β-amylase from sweet potato (*2*). In the case of n-BSA, multiple attack action has been recognized qualitatively using ^{14}C-labeled maltoheptaose (G7) (*32*). We examined the multiple attack action using G7 by HPLC. Figure 2 shows the distribution of products from G7 with n-SBA. The apparent action pattern is the same as that observed for β-amylase from sweet potato (*2*). Any differences among n-SBAs (isozymes) and recombinant SBA (r-SBA) were not observed (Figure 2). On analysis of the products, a significant multiple attack action was confirmed for wild-type SBA (both n-SBA and r-SBA). The values (P0 and P5/P7) which are used for estimation of multiple attack (Figure 1) are calculated with the previous

Table 1: Probabilities for SBAs When the Substrate Is G7[a]

	P0	P5/P7
wild-type SBA	0.55 ± 0.01	1.00 ± 0.01
D53A	0.17 ± 0.01	0.79 ± 0.01
W55R	0.00 ± 0.01	0.69 ± 0.01

[a] Numerical values of P0 and P5/P7 (Figure 1) were determined with the method described previously (*24*).

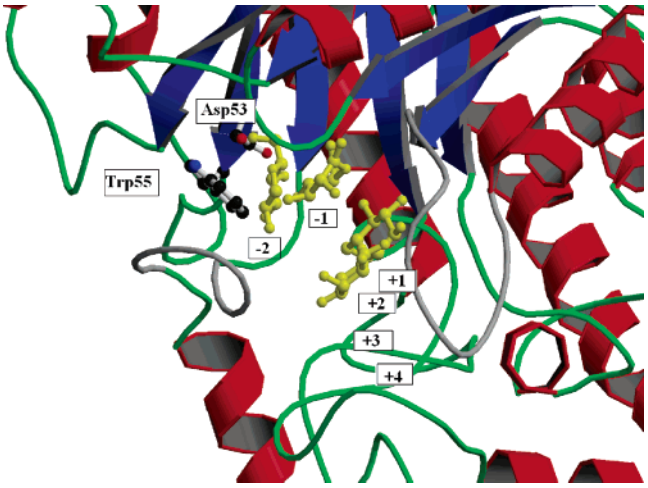

FIGURE 3: Overall structure of SBA and the maltose complex (1BFN). Maltose (yellow), Asp53, and Trp55 located at the active site are shown in ball and stick representation. The catalytic site is located between subsites −1 and +1. Subsites are numbered from the catalytic site.

Table 2: Kinetic Parameters for SBAs for Reduced Soluble Starch[a]

	k_{cat} (s^{-1})	K_m (μM)	k_{cat}/K_m ($s^{-1}\,\mu M^{-1}$)
SBA	(12 ± 1) × 10^6	770 ± 10	(0.16 ± 0.08) × 10^5
D53A	(2.0 ± 0.2) × 10^6	1020 ± 130	(0.20 ± 0.03) × 10^4
W55R	(4.6 ± 0.5) × 10^6	1520 ± 150	(0.30 ± 0.04) × 10^4

[a] Kinetic parameters for the hydrolytic activity of SBAs were examined using reduced soluble starch at pH 5.7 and 40 °C with the method described previously (*31*).

method (Monte Carlo simulation) (Table 1) (*24*). The theoretical lines from the Monte Carlo simulation were well fitted to the observed data (Figure 2). P0 is the probability of sliding and is estimated to be 0.55. P5/P7 is the ratio for the probability of forming a "productive complex" with G5 and G7 (Figure 1) and is estimated to be 1.00. This value means that the affinity of subsite +4 in wild-type SBA is negligible.

Product Distribution from G7 by Mutant SBAs. From the structure of the complex of SBA and maltose (*17*), it was proven that Asp53 is located at the edge of the substrate binding site (subsite −2) and contributes to the hydrogen-bonding interaction between the residues and carbohydrate ligand in SBA (Figure 3). Trp55 is also located near the substrate binding site (subsite −2) and close to Asp53 (Figure 3). These residues are located about 8 Å away from the active center. In order to determine the role of Asp53 and Trp55 at subsite −2 for multiple attack, we prepared mutant SBAs in which Asp53 and Trp55 were changed to Ala (D53A) and Arg (W55R), respectively. The activities toward soluble starch were reduced by the mutations (Table 2). However, there was a little difference in the K_m values. By changing Asp55 to Ala (D53A), the carboxyl residue can be removed

Table 3: Data Collection Statistics of the SBA Mutant (W55R)[a]

X-ray source	BL24XU (SPring8)
detector	RIGAKU R-AXIS4
temperature (K)	100
wavelength (Å)	0.835
exposure time (s)	600
resolution range (Å)	19.96−2.20 (2.23−2.20)
space group	$P3_121$
cell parameters (Å)	$a = b = 85.04$, $c = 145.08$
no. of observed reflections	307911 (4193)
no. of unique reflections	34130 (994)
completeness (%)	98.9 (98.9)
R_{merge}[b] (%)	7.4 (15.8)
protein atoms in refinement	3921
water molecules in refinement	327
average *B*-factor (Å^2)	11.7
bond length rmsd (Å)	0.00599
bond angle rmsd (deg)	1.30
R[c] (%)	20.5
R_{free}[d] (%)	25.2

[a] The values in the shell at highest resolution are shown in parentheses. [b] $R_{merge} = \sum_h\sum_i|I(h)_i - \langle I(h)\rangle|/\sum_h\sum I(h)_i$, where $I(h)$ is the intensity measurement of refrections and $\langle I(h)\rangle$ is the mean value of $I(h)_i$ for all i measurements. [c] $R = \sum_h||F_o| - |F_c||/\sum_h|F_o|$, where F_o and F_c are the observed and calculated structure factor amplitudes, respectively. [d] R_{free} is calculated with 5% of the diffraction data, which were not used during the refinement.

from Asp53. The activities of D53A and W55R toward G7 substrate were decreased to 13% and 20% of those of wild-type SBA, respectively. Figure 4 shows action patterns of the distribution of products from G7 with D53A (Figure 4A) and W55R (Figure 4B). On comparison with the wild-type SBA (Figure 2), it is clear that the production of G3 at the first stage was decreased and the production of G5 was increased by these mutations. The P0 and P5/P7 values for D53A (Figure 4A) were determined to be 0.17 and 0.79, respectively (Table 1). The P0 and P5/P7 values for W55R (Figure 4B) were determined to be 0 and 0.69, respectively (Table 1). This means that the multiple attack action of SBA decreased and completely disappeared by changing Asp53 to Ala and Trp55 to Arg, respectively. It was suggested that the carboxyl residue of Asp53 contributed to the expression of amylase activity. The carboxyl residue of Asp53 was also important for multiple attack action. Trp55 is not located at the substrate binding site. Therefore, the effect of Trp55 is not indispensable for the amylase activity but crucial for the multiple attack action. The mutant enzyme (W55R) represents the first instance of mutation that abolished processivity without significant impact on catalysis. The dependency of the enzyme concentration (W55R) was not observed (Figure 4B). The result that the P5/P7 value was changed to 0.79 or 0.69 (Table 1) indicates that subsite +4 obtains some affinity toward the substrate (Figure 1) by these mutations. In order to understand the function of Trp55, we analyzed the crystal structure of W55R.

Crystal Structure of W55R. In order to elucidate the structure of the active site, we prepared a crystal and solved the crystal structure of W55R in the resolution range of 19.96−2.2 Å. The rigid body fitting indicated that the root mean square difference of Cα atoms (residues 8−494) between the wild-type SBA (PDB code 1WDP) and W55R was 0.215 Å. This indicates that the wild-type SBA and W55R have the same structure except for the mutation site. Figure 5 provides a detailed comparison at the active site between wild-type SBA and W55R. The carboxyl residue

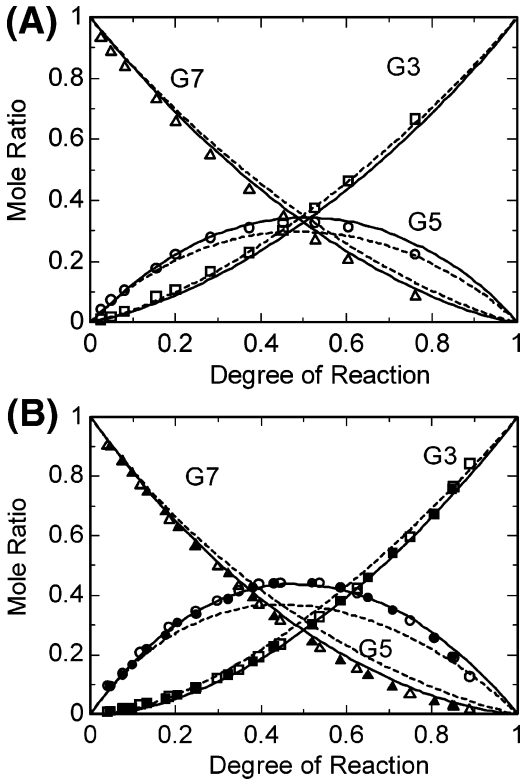

FIGURE 4: Experimental and simulation data of the product distribution (G5 and G3) from D53A (A) and W55R (B). The horizontal and vertical coordinates are defined as in Figure 2. Experimental points are G3 (square), G5 (circle), and G7 (triangle). □, ○, and △ are the data for D53A (5.01 milliunits/mL) (A) and W55R (15.2 milliunits/mL) (B). ■, ●, and ▲ are the data for W55R (49.0 milliunits/mL) (B). Solid lines are best-fitted simulated data using P0 = 0.17 (A) and 0.00 (B) and (P5/P7) = 0.79 (A) and 0.69 (B), respectively (Table 1). The broken lines are theoretical lines using the best-fit value of P0 [P0 = 0.17 (A) and P0 = 0.00 (B)] keeping P5/P7 = 1.00, assuming that subsite +4 does not exist.

of Asp53 in wild-type SBA is located at the surface of the substrate binding site (subsite −2) and 6−9 Å away from the active center (Glu186 and Glu380) (Figure 3). By changing Trp55 to Arg, the direction of the carboxyl residue of Asp53 changed. The carboxyl residue of Asp53 rotated about 120° along the Cα−Cβ bond and the carboxyl O atom of Asp53 formed a hydrogen bond with the Nϵ atom of Arg55 in W55R (Figure 5). Figure 6 shows the superimposition of wild-type SBA complexed with maltose (PDB code 1BFN) and W55R at the active site. The bound maltose molecules were found at subsites −2 to −1 and subsites +1 to +2 for wild-type SBA. The carboxyl O atom of Asp53 forms a hydrogen bond to the O4 and O6 atoms of Glc (−2) in wild-type SBA (Figure 6). The position of Trp55 is over 3.6 Å away from the O3 and O4 atoms of Glc (−2). The carboxyl O atom of Asp53 is difficult to make the hydrogen bond with the O3 and O4 atoms (5.3−5.9 Å away from the carboxyl O atom of Asp53) of Glc (−2) in W55R (Figures 5 and 6), due to forming a hydrogen bond with the Nϵ atom of Arg55. The other residues in the active site were not influenced by this mutation.

DISCUSSION

In the case of the action pattern of SBA with G7 as the substrate, the theoretical lines with P0 = 0.55 and P5/P7 = 1.00 were well fitted to the observed values (Figure 2). P5/

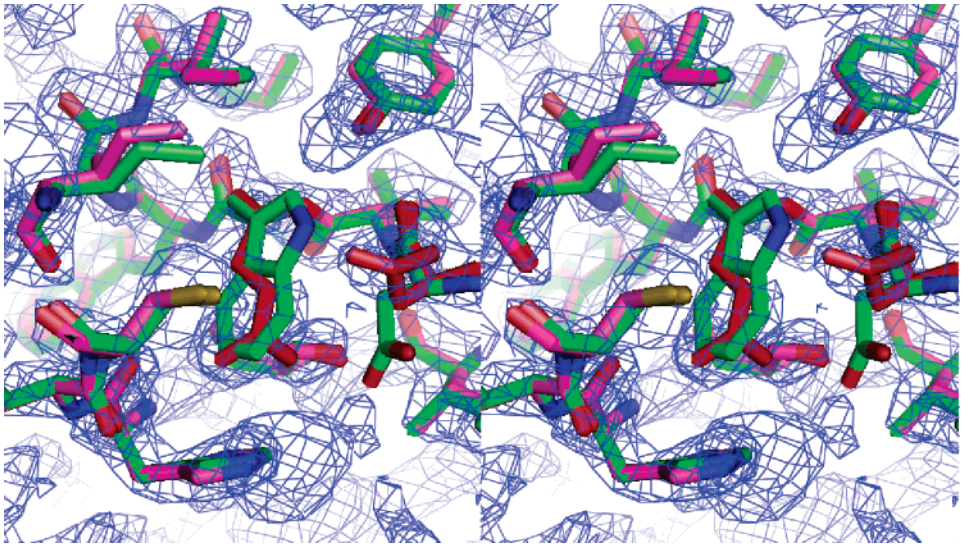

FIGURE 5: Stereoview (wall-eyed) of $2F_o - F_c$ electron density map and modeled W55R (pink and red) at subsite −2. Superimposed wild-type SBA is shown in green. Note that the position of the carboxyl residue of Asp53 (red) is changed by Arg55 (red).

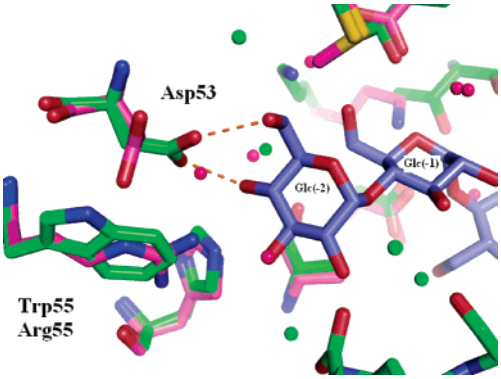

FIGURE 6: Superimposed wild-type SBA (green) and W55R (pink) at the active site. Maltose bound to wild-type SBA at subsites −2 and −1 is represented in blue. The hydrogen bonds between the carboxyl O atom of Asp53 and Glc (−2) in wild-type SBA are shown as dotted lines. The distances between O atoms of C6 and C4 in maltose and O atoms of the carboxyl residue of Asp53 in W55R are over 5 Å.

P7 corresponds to the ratio of the binding constants of G5 and G7 (Figure 1). P5/P7 = 1.00 shows that subsite +4 has no effect on the action pattern of SBA (Figure 1). In the action pattern of SBA with the calculated values, it is expected that 1.55 and 2.22 molecules of G2 are released from a single E−S complex with G7 and an infinitely long oligosaccharide, respectively. From the highly conserved sequence similarity and structure of β-amylase from plants (*19*, *33*), the multiple attack action must be in common for β-amylases from plants. In the case of β-amylases from microorganisms (which exhibit a little homology to those from plants), investigation upon the multiple attack action is not reported.

Although Trp55 is not located in the active center of SBA (*17*), the action pattern of W55R completely changed. The present finding that the theoretical lines with P0 = 0.00 and P5/P7 = 0.69 for W55R were well fitted to the observed values (Figure 4B) indicates that one point mutation leads to extreme reduction of the multiple attack action with significant hydrolytic activity. It was elucidated that Trp55 plays a critical role in the multiple attack mechanism. Although there is a possibility that other factors are indispensable for the multiple attack action, this residue must be one of the important factors for the multiple attack. When simulation of the multiple attack action for W55R was carried out without subsite +4, the theoretical lines changing only the parameter P0 did not fit the observed values [keeping P5/P7 = 1, as shown (Figure 4B)]. The affinity of subsite +4 has some effect on the action pattern of SBA (Figure 1). The different values of P5/P7 between SBA and W55R (Table 1) suggest some correlation between subsites −2 and +4 of the enzyme. In the case of D53A, the theoretical lines with P0 = 0.17 and P5/P7 = 0.79 were well fitted to the observed values (Figure 4A). These values are between those of the wild-type SBA and W55R. It was reported that some mutant enzymes exhibited a qualitatively decreased multiple attack with a small hydrolytic activity (*30*). And it had been speculated that the additional substrate binding at the reducing end of the substrate or stable E−P complex was related to the hydrolytic activity and multiple attack (*10*, *29*, *30*). But the values of W55R (Tables 1 and 2) indicate that the enzyme without multiple attack action exhibited significant hydrolytic activity. The effect of Trp55 is not indispensable for the amylase activity but crucial for the multiple attack action.

Generally, an enzyme holds a substrate (or product) through weak interactions before and after forming a stable E−S or E−P complex (*34*). In the case of SBA, it is assumed that a long-chain substrate and products can slide easily along the catalytic binding cleft of the enzyme (*2*, *29*, *31*), since many kinds of hydrophobic and van der Waals interactions have been recognized in the E−S complex of SBA (*17*). Before or after release of the product, there is a possibility to form the new productive E−S complex exchanging weak hydrophobic and van der Waals interactions. In the case of wild-type SBA, the probability of multiple attack (P0 = 0.55) is higher than that of dissociation (1 − P0 = 0.45). Furthermore, the data suggest that the action of multiple attack needs the suitable stabilization of the substrate by Asp53 through the nonreducing end of the substrate. Too strong interactions between them inhibit the release of the G2 product and disturb the multiple attack action as a result. The inhibition phenomena were observed in the case of the

specific inhibitors that can bind at subsites −1 and −2 (*6*, *35*).

Structual analysis of W55R supports that extreme reduction of the multiple attack action of W55R is mainly due to the change in the direction of the carboxyl residue of Asp53. The position of the carboxyl residue of Asp53 was changed by the positively charged residue at Arg55, and the binding affinity of subsite −2 was reduced. The phenomena of the weak multiple attack action of D53A seem to depend on the weak interaction, such as van der Waals, among two residues (Ala53 and Trp55) and the substrate. Changing the direction of the carboxyl residues is a better method for reducing the multiple attack action in comparison with the deletion of the target residue. At the nonreducing end binding site, Asp53 and His93 of SBA are related to the hydrogen bonding to the O4 atom of Glc (−2) (*17*). However, His93 alone is not enough for productive binding. The change in P5/P7 is due to the change in binding free energy between glucose and subsite +4 (Figure 1, Table 1). The finding that the binding affinity for subsite +4 is influenced by subsite −2 (Table 1) suggests that the affinity of each subsite is not independent. The dependency of subsites must be strongly related to the substrate sliding into the cleft of the enzyme.

From the sequence alignment, it was clarified that the sequence around Asp53, Trp55, and His93 is well conserved among plants and microorganisms (*19*). Therefore, the roles of these residues in the hydrolytic mechanism seem to be common for β-amylases. We can propose two important factors for the multiple attack action. One of them is the relative sliding from the nonproductive binding mode and the other is the factor stabilizing the productive binding mode. When the nonreducing end glucose is not stabilized around subsite −2, the multiple attack action is disturbed. The structure around Asp53 and His93 and the multiple attack action of β-amylase must evolve to produce G2 effectively from native substrate. Other amino acid residues stabilizing the glucose residue at subsite −2 may have a similar function as Asp53.

The sliding or processive action of a protein along a DNA chain seems to be a similar phenomenon to be present in the multiple attack mechanism. The sliding has been confirmed kinetically and visually (*12*−*14*, *36*). Sliding and dissociation are competitive pathways, as observed for β-amylases. The main nonspecific binding, which is important for the sliding, is thought to be an electrostatic interaction between a protein and DNA. The hydrogen bonds between them also play an important role in the sliding for endonuclease (*13*). But strong hydrogen bonds between DNA and a protein inhibit the smooth sliding. The relevant combinations of van der Waals interactions and hydrogen bonds between proteins and polymer chains are important for an effective search for its target site. In the case of β-amylases, a substrate slides by just the maltose unit, and the proper position is fixed by the hydrogen bonding, as observed in the case of DNA binding protein. In the case of SBA, water molecules at the active site form a hydrogen-bonding network, and these water molecules can be replaced by the substrate (*37*, *38*). These many water molecules seem to play a significant role for the polymer sliding along the cleft of β-amylases although dynamic roles of hydrated water molecules are not clear at present.

ACKNOWLEDGMENT

We thank Dr. Kazuaki Harata (National Institute of Advanced Industrial Science and Technology) for helpful advice and members of Dr. Fukazawa's group for technical assistance.

REFERENCES

1. Bailey, J. M., and French, D. (1957). The significance of multiple reactions in enzyme polymer systems, *J. Biol. Chem. 226*, 1−14.
2. French, D., and Youngquist, R. W. (1963). Die Wirkungsweise von beta-amylase auf Starkeoligosaccharide, *Starke 12*, 425−431.
3. Robyt, J. F., and French, D. (1967). Multiple attach hypothesis of alpha-amylase action: action of porcine pancreatic, human salivary, and *Aspergillus Oryzae* alpha-amylases, *Arch. Biochem. Biophys. 122*, 8−16.
4. Thoma, J. A., Brothers, C., and Spradlin, J. (1970). Subsite mapping of enzymes. Studies on *Bacillus subtilis* amylase, *Biochemistry 9*, 1768−1775.
5. Thoma, J. A., Rao, G. V., Brothers, C., Spradlin, J., and Li, L. H. (1971). Subsite mapping of enzymes. Correlation of product patterns with Michaelis parameters and substrate-induced strain, *J. Biol. Chem. 246*, 5621−5635.
6. Thoma, J. A. (1976). Models for depolymerizing enzymes: criteria for discrimination of models, *Carbohydr. Res. 48*, 85−103.
7. Mazur, A. K., and Nakatani, H. (1993). Multiple attack mechanism in the porcine pancreatic alpha-amylase hydrolysis of amylose and amylopectin, *Arch. Biochem. Biophys. 306*, 29−38.
8. Kleman-Leyer, K. M., Siika-Aho, M., Teeri, T. T., and Kirk, T. K. (1996). The cellulases endoglucanase I and cellobiohydrolase II of *Trichoderma reesei* act synergistically to solubilize native cotton cellulose but not to decrease its molecular size, *Appl. Environ. Microbiol. 62*, 2883−2887.
9. Arai, T., Araki, R., Tanaka, A., Karita, S., Kimura, T., Sakka, K., and Ohmiya, K. (2003). Characterization of a cellulase containing a family 30 carbohydrate-binding module (CBM) derived from *Clostridium thermocellum* CelJ: importance of the CBM to cellulose hydrolysis, *J. Bacteriol. 185*, 504−512.
10. Uchiyama, T., Katouno, F., Nikaidou, N., Nonaka, T., Sugiyama, J., and Watanabe, T. (2001). Roles of the exposed aromatic residues in crystalline chitin hydrolysis by chitinase A from *Serratia marcescens* 2170, *J Biol. Chem. 276*, 41343−41349.
11. Watanabe, T., Ariga, Y., Sato, U., Toratani, T., Hashimoto, M., Nikaidou, N., Kezuka, Y., Nonaka, T., and Sugiyama, J. (2003). Aromatic residues within the substrate-binding cleft of *Bacillus circulans* chtinase A1 are essential for hydrolysis of crystalline chitin, *Biochem. J. 376*, 237−244.
12. Kabata, H., Kurosawa, O., Arai, I., Washizu, M., Margarson, S. A., Glass, R. E., and Shimamoto, N. (1993). Visualization of single molecules of RNA polymerase sliding along DNA, *Science 262*, 1561−1563.
13. Jeltsch, A., Wenz, C., Stahl, F., and Pingoud, A. (1996). Linear diffusion of the restriction endonuclease EcoRV on DNA is essential for the in vivo function of the enzyme, *EMBO J. 15*, 5104−5111.
14. van Noort, S. J., van der Werf, K. O., Eker, A. P., Wyman, C., de Grooth, B. G., van Hulst, N. F., and Greve, J. (1998). Direct virualization of dynamic protein-DNA interactions with a dedicated atomic force microscope, *Biophys. J. 74*, 2840−2849.
15. Isoda, Y., and Nitta, Y. (1986). Affinity labeling of soybean beta-amylase with 2′,3′-epoxypropyl alpha-D-glucopyranoside, *J. Biochem. (Tokyo) 99*, 1631−1637.
16. Mikami, B., Hehre, E. J., Sato, M., Katsube, Y., Hirose, M., Morita, Y., and Sacchettini, J. C. (1993). The 2.0-Å resolution structure of soybean beta-amylase complexed with alpha-cyclodextrin, *Biochemistry 32*, 6836−6845.
17. Mikami, B., Degano, M., Hehre, E. J., and Sacchettini, J. C. (1994). Crystal structures of soybean beta-amylase reacted with beta-maltose and maltal: active site components and their apparent roles in catalysis, *Biochemistry 33*, 7779−7787.
18. Nanmori, T., Nagai, M., Shimizu, Y., Shinke, R., and Mikami, B. (1993). Cloning of the beta-amylase gene from *Bacillus cereus* and characteristics of the primary structure of the enzyme, *Appl. Environ. Microbiol. 59*, 623−627.
19. Pujadas, G., Ramirez, F. M., Valero, R., and Palau, J. (1996). Evolution of beta-amylase: patterns of variation and conservation

in subfamily sequences in relation to parsimony mechanisms, *Proteins 25*, 456−472.
20. Oyama, T., Kusunoki, M., Kishimoto, Y., Takasaki, Y., and Nitta, Y. (1999). Crystal structure of beta-amylase from *Bacillus cereus* var. mycoides at 2.2 Å resolution, *J. Biochem. (Tokyo) 125*, 1120−1130.
21. Mikami, B., Yoon, H. J., and Yoshigi, N. (1999). The crystal structure of the sevenfold mutant of barley beta-amylase with increased thermostability at 2.5 Å resolution, *J. Mol. Biol. 285*, 1235−1243.
22. Totsuka, A., Nong, V. H., Kadokawa, H., Kim, C. S., Itoh, Y., and Fukazawa, C. (1994). Residues essential for catalytic activity of soybean beta-amylase, *Eur. J. Biochem. 221*, 649−654.
23. Nakatani, H. (1996). Monte Carlo simulation of multiple attack mechanism of alpha-amylase, *Biopolymers 39*, 665−669.
24. Nakatani, H. (1997). Monte Carlo simulation of multiple attack mechanism of beta-amylase-catalyzed reaction, *Biopolymers 42*, 831−836.
25. Totsuka, A., and Fukazawa, C. (1993). Expression and mutation of soybean beta-amylase in *Escherichia coli*, *Eur. J. Biochem. 214*, 787−794.
26. Wang, Y., Arahira, M., and Fukazawa, C. (1999). An isoelectric separation of soybean beta-amylase isoforms and their enzymatic characteristics, *Biosci. Biotechnol. Biochem. 63*, 726−730.
27. Roussel, A., and Cambillau, C. (1991) Turbo Frodo, in *Silicon Graphics Geometry Partners Directory*, Silicon Graphics, Mountain View, CA.
28. Brunger, A. T., Adams, P. D., Clore, G. M., DeLano, W. L., Gros, P., Grosse-Kunstleve, R. W., Jiang, J. S., Kuszewski, J., Nilges, M., Pannu, N. S., Read, R. J., Rice, L. M., Simonson, T., and Warren, G. L. (1998). Crystallography & NMR system: A new software suite for macromolecular structure determination, *Acta Crystallogr., Sect. D: Biol. Crystallogr. 54* (Part 5), 905−921.
29. Adachi, M., Mikami, B., Katsube, T., and Utsumi, S. (1998). Crystal structure of recombinant soybean beta-amylaser complexed with beta-cyclodextrin, *J. Biol. Chem. 273*, 19859−19865.
30. Kang, Y. N., Tanabe, A., Adachi, M., Utsumi, S., and Mikami, B. (2005). Structural analysis of threonine 342 mutants of soybean beta-amylase: role of a conformational change of the inner loop in the catalytic mechanism, *Biochemistry 44*, 5106−5116.
31. Totsuka, A., and Fukazawa, C. (1996). Functional analysis of Glu380 and Leu383 of soybean beta-amylase. A proposed action mechanism, *Eur. J. Biochem. 240*, 655−659.
32. Suganuma, T., Mizukami, T., Moori, K., Ohnishi, M., and Hiromi, K. (1980). Studies of the action pattern of an alpha-amylase from *Streptomyces praecox* NA-273, *J. Biochem. (Tokyo) 88*, 131−138.
33. Cheong, C. G., Eom, S. H., Chang, C., Shin, D. H., Song, H. K., Min, K., Moon, J. H., Kim, K. K., Hwang, K. Y., and Suh, S. W. (1995). Crystallization, molecular replacement solution, and refinement of tetrameric beta-amylase from sweet potato, *Proteins 21*, 105−117.
34. Hammes, G. G., and Schimmel, P. R. (1970) *The Enzymes (3rd Ed.*), 67−114.
35. Banks, W., Greenwood, C. T., and Khan, K. M. (1971). Studies on starch-degrading enzymes. XIV. The multiple forms of procine, pancreatic alpha-amylase, *Carbohydr. Res. 20*, 233−242.
36. Richter, P. H., and Eigen, M. (1974). Diffusion controlled reaction rates in spheroidal geometry. Application to repressor-operator association and membrane bound enzymes, *Biophys. Chem. 2*, 255−263.
37. Laederach, A., Dowd, M. K., Coutinho, P. M., and Reilly, P. J. (1999). Automatic docking of maltose, 2-deoxymaltose, and maltotetraose into the soybean beta-amylase active site, *Proteins 37*, 166−175.
38. Pujadas, G., and Palau, J. (2001). Molecular mimicry of substrate oxygen atoms by water molecules in the beta-amylase active site, *Protein Sci. 10*, 1645−1657.

BI061605W